Determining AC Magnetic Susceptibility of Kilogram-Level Test Masses for TianQin

Jia-Hao Xu[1,2], Wen-Long Ma[1], Ya-Ting Zhang[3*], Qing-Lan Wang[4], Lin Zhu[5], and Qi Liu[2*]

[1]*Faculty of Information Engineering, Quzhou College of Technology, Quzhou 324000, China*
[2]*TianQin Research Center for Gravitational Physics & School of Physics and Astronomy, Ministry of Education Key Laboratory of TianQin Mission, Frontiers Science Center for TianQin, Gravitational Wave Research Center of CNSA, Sun Yat-sen University (Zhuhai Campus), Zhuhai 519082, China*
[3]*School of Physics and Electronic Engineering, Hubei Key Laboratory of Low Dimensional Optoelectronic Materials and Devices, Hubei University of Arts and Science, Xiangyang 441053, China*
[4]*School of Mathematics, Physics and Optoelectronic Engineering, Hubei University of Automotive Technology, Shiyan 442002, China*
[5]*Ministry of Education Key Laboratory of Fundamental Physical Quantities Measurement, Hubei Key Laboratory of Gravitation and Quantum Physics, Precision Gravity Measurement Facility and School of Physics, Huazhong University of Science and Technology, Wuhan 430074, China*

(Received 23 March 2025; accepted manuscript online 15 May 2025)

The effect from the interaction of the alternating current (AC) magnetic field with kilogram-level test mass (TM) limits the detectivity of the TianQin space-based gravitational wave detection. The quantified effect requires the determination of the AC magnetic susceptibility $\chi(f)$ of the TM. A torque method is proposed to measure the $\chi(f)$ of kg-level samples at the mHz band with a precision of 1×10^{-7}. Combined with our previous work [*Phys. Rev. Appl.* **18** 044010 (2022)], the general frequency-dependent susceptibility of the alloy cube with side length L and electrical conductivity σ is determined as $\chi(f) = \chi_0 + (0.24 \pm 0.01)\sigma\mu_0 L^2 f$ from 0.1 mHz to 1 Hz. The determination is helpful for the preliminary estimation of the in-band eddy current effect in the TianQin noise budget. The technique can be adopted to accurately measure $\chi(f)$ of the actual TM in other precision experiments, where the magnetic noise is a significant detection limit.

DOI: 10.1088/0256-307X/42/7/071101 CSTR: 32039.14.0256-307X.42.7.071101

1. Introduction. Space-based gravitational wave (GW) detection provides a unique tool for testing gravity and opens a groundbreaking low-frequency observation window for astronomy and cosmology.[1–4] It relies on three identical spacecraft, which are placed on identical geocentric or heliocentric orbits to construct nearly equilateral triangle constellations. Inter-spacecraft laser interferometry is used to monitor the distances between the free-falling test masses (TMs) inside the drag-free spacecraft. These TMs are identical Au–Pt alloy cubes with a side length of about 5 cm and a weight of about 2.45 kg in TianQin GW detection.[5] The TMs are expected to follow their geodesic trajectories, or in other words, to work in pure free-falling mode, which is one of the most challenging technologies needed for the space-based GW mission.[6,7] The requirement of residual acceleration noise $a_{\rm n}$ in TianQin detection should be kept below $1\,{\rm fm\cdot s^{-2}\cdot Hz^{-1/2}}$ at mHz.[8]

The time-varying magnetic field $B(\omega)$ will produce eddy currents inside the TMs, and then induce a magnetic moment expressed as $\chi(\omega)V\mu_0^{-1}B(\omega)$, where V is the volume of the TM and μ_0 is the magnetic permeability. The complex number $\chi(\omega)$ is the alternating current (AC) volume susceptibility, which is a general characterization of the induction under the uniform magnetic field,[9] namely, the uniform time-varying interplanetary magnetic field from 0.1 mHz to 1 Hz in space-based GW detection.[10] Then, this time-varying induced magnetic moment will couple with the constant (DC) spacecraft magnetic field gradient $\nabla B_{\rm DC}$ and hence produce a magnetic force noise, which can be calculated by $F_{\rm e} = [\chi(\omega)V\mu_0^{-1}B(\omega)\cdot\nabla]B_{\rm DC}$.[11,12] Since $B(\omega)$ is in the band of the GW detection, the force noise will contribute to the $a_{\rm n}$ directly. This in-band effect is a dominant part of the magnetic noise in the low-frequency regime.[13]

In LISA GW detection, the contribution of this effect to $a_{\rm n}$ will be less than 10% thanks to the good magnetic field environment in a heliocentric orbit and the well-prepared Au–Pt alloy TM.[13] Unlike LISA, the TianQin spacecraft operate on a geocentric orbit, and the TM would be subject to a stronger influence of the magnetic fields from the Earth and the Moon. In the preliminary concept of TianQin, the contribution of this effect to $a_{\rm n}$ should be less than $0.24\,{\rm fm\cdot s^{-2}\cdot Hz^{-1/2}}$.[5] The magnetic effect is one of the significant interfering factors in TianQin, where the budgets of each interfering factor are stringent. Hence, accurate estimation of this effect is crucially important for

*Corresponding authors. Email: zhangyating@hbuas.edu.cn; liuq239@sysu.edu.cn
© 2025 Chinese Physical Society and IOP Publishing Ltd. All rights, including for text and data mining, AI training, and similar technologies, are reserved.

TianQin.

In order to quantitatively estimate this in-band eddy current effect $F_{\rm e}$ in the TianQin GW detection band from 0.1 mHz to 1 Hz, it is necessary to precisely measure the AC susceptibility $\chi(\omega)$ of a kg-level TM within the band. Recently, LISA measured the TM $\chi(\omega)$ from 2 mHz to 30 mHz with a precision of 10^{-6} in the LISA Pathfinder (LPF) on-orbit measurements.[14] Traditional instruments based on fluxmetric measurement, such as the induced bridge, MPMS, and PPMS, are inapplicable due to the small specimen chamber[15] or the limited measurement frequency above 0.1 Hz.[16,17] Other specialized instruments applied in space-based GW detection to measure the magnetic properties of TM, such as the torsion pendulums, are focused on the precision measurement of the static magnetic properties.[18–21]

In our previous work, we developed a method based on a torsion pendulum to measure the $\chi(\omega)$ of a 2-cm-size cube copper sample with a weight of approximately 70 g.[22] The actual TMs applied in GW detection are 5-cm-size Au–Pt alloy cubes with a weight of approximately 2.45 kg. Accurate determination of the $\chi(\omega)$ of the actual TM requires multiple comparative experiments with different samples, rather than relying solely on the AC susceptibility data of a single 2-cm-size copper sample. This is because the AC susceptibility depends not only on the material of the TM but also on other properties such as conductivity, size, and shape. Thus, for quantitatively estimating this eddy current effect in GW detection, the new technique for measuring the $\chi(\omega)$ of kg-level cube TMs within the band needs to be investigated.

2. Method and Instrument. The induced magnetic moment $\boldsymbol{m}_{\rm i}$ of an isotropic TM in a space-uniform and time-invariant magnetic field $\boldsymbol{B}$ will not produce a magnetic torque, since the vector $\boldsymbol{m}_{\rm i} \sim \chi\boldsymbol{B}$ is always parallel to $\boldsymbol{B}$.[23] Here, a space-uniform but time-varying magnetic field $\boldsymbol{B} = B_x(\omega)\hat{\boldsymbol{x}} + B_y\hat{\boldsymbol{y}}$ is applied to the TM,

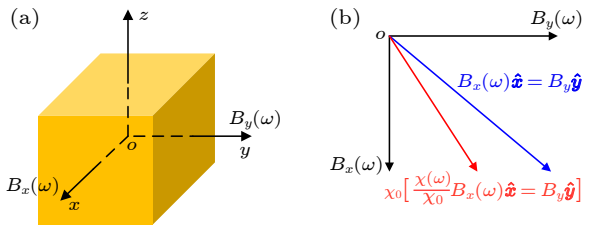

Fig. 1. (a) Schematic diagram of the magnetic field applied to the TM. The yellow cube is the TM. The origin of the coordinate system is located at the center of the TM, and the horizontal coordinates are parallel to the sides of the cube, respectively. A space-uniform and time-varying field $B_x(\omega)\hat{\boldsymbol{x}}$ is applied to the TM along the x-axis, and a space-uniform constant field $B_y\hat{\boldsymbol{y}}$ is applied to the TM along the y-axis. (b) The time-varying coordinate relation between the field and the induced magnetic moment at one time point. The blue vector denotes the superimposed field of $B_x(\omega)\hat{\boldsymbol{x}}$ and $B_y\hat{\boldsymbol{y}}$. The red vector denotes the superimposed induced magnetic moment of the $\chi(\omega)B_x(\omega)\hat{\boldsymbol{x}}$ and $\chi_0 B_y\hat{\boldsymbol{y}}$. The superimposed field (blue vector) and the superimposed induced magnetic moment (red vector) are not parallel.

where $B_x(\omega)\hat{\boldsymbol{x}}$ is the space-uniform magnetic field with frequency ω, and $B_y\hat{\boldsymbol{y}}$ is the constant space-uniform magnetic field, as shown on the left in Fig. 1. The induced magnetic moment along the x- and y-axes is $\chi(\omega)B_x(\omega)\hat{\boldsymbol{x}}$ and $\chi_0 B_y\hat{\boldsymbol{y}}$, respectively. If the AC susceptibility $\chi(\omega)$ is not equal to the static (DC) susceptibility χ_0, the induced magnetic moment $\chi(\omega)B_x(\omega)\hat{\boldsymbol{x}} + \chi_0 B_y\hat{\boldsymbol{y}}$ will no longer be parallel to $\boldsymbol{B} = B_x(\omega)\hat{\boldsymbol{x}} + B_y\hat{\boldsymbol{y}}$, as shown on the right in Fig. 1. Then the TM will sense a nonzero induced torque $N_{\rm i}(\omega)$ along the z-axis which can be written as

$$\begin{aligned} N_{\rm i}(\omega) &= [\chi(\omega)V\mu_0^{-1}B_x(\omega)]B_y - [\chi_0 V\mu_0^{-1}B_y]B_x(\omega) \\ &= [\chi(\omega) - \chi_0]B_x(\omega)B_y V\mu_0^{-1}, \end{aligned} \tag{1}$$

where the DC susceptibility χ_0 can be measured by a traditional torsion pendulum.[22] The nonzero factor $\chi(\omega) - \chi_0$ in Eq. (1) implies the difference in the induced process of TM at magnetic fields with different time-domain features. The different time-domain features of magnetic fields break the isotropic susceptibility of the TM. In this way, the $\chi(\omega)$ can be measured.

In laboratory measurement, the environmental magnetic field component $B_{{\rm E}y}$ along the y-axis should be added to the artificial component B_y, and thus the total B_y should be replaced by $B_y + B_{Ey}$ in Eq. (1). Similarly, the intrinsic remanent magnetic moment of TM m_{ry} along the y-axis will mix into the induced moment $\chi_0(B_y + B_{{\rm E}y})V$, which contributes to a disturbed torque. The remanent moment m_{ry} of the TM was measured to be approximately 10 nA·m^2.[15] The m_{ry} will interact with the field $B_x(\omega)$, and then contribute a disturbance torque $m_{ry}B_x(\omega) \approx 1$ pN·m with the typical amplitude of the $B_x(\omega)$ about 100 μT. The disturbance torque is at the same level as the noise floor of the torsion pendulum, and hence can be ignored. Hence, the Eq. (1) can be rewritten as

$$N_{\rm i}(\omega) = [\chi(\omega) - \chi_0]B_x(\omega)B_Y V\mu_0^{-1}, \tag{2}$$

where $B_Y = B_y + B_{{\rm E}y}$ is the total magnetic field component along the y-axis.

The schematic drawing of the measuring instrument is shown in Fig. 2. The TM, a 1.3 kg copper (99.9999% purity) cube, is suspended by a 60-cm-long and 125-μm-diameter tungsten fiber to form a torsion pendulum. This tungsten fiber is sufficient to load the torsion pendulum, since the load capacity of the fiber is about 2.5 kg,[24,25] which is larger than the required load capacity. A small circular mirror used for optical readout of the pendulum's rotational angle is attached at the center of one face of the TM. Two Helmholtz coils are installed along two orthogonal directions around the TM to produce an artificial uniform magnetic field $\boldsymbol{B} = B_x(\omega)\hat{\boldsymbol{x}} + B_y\hat{\boldsymbol{y}}$. The artificial field uniformity in the TM space of the x-axis and the y-axis is 2.7% and 1.5%, respectively.

The entire device is installed in a vacuum chamber maintained at a pressure of 10^{-5} Pa by an ion pump during the whole experiment. The twist angle of the pendulum $\theta(t)$ is monitored by an autocollimator that reflects the light off the small reflector. The natural resonant frequency f_0 of the pendulum,

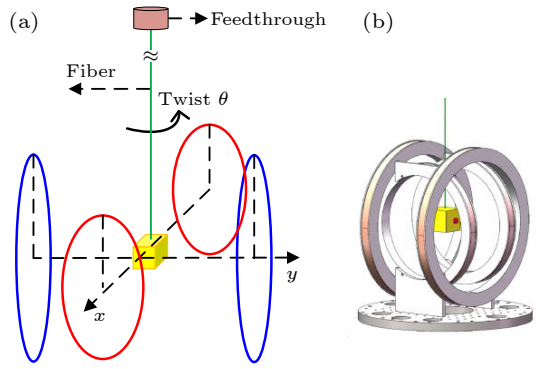

Fig. 2. Schematic diagram of the device. (a) The yellow cube is the TM, which is suspended by the lower end of the 125-μm fiber. The upper end of the fiber is linked with the feedthrough mounted on top of the vacuum chamber. The TM and the fiber form the torsion pendulum, and the pendulum can rotate around the fiber with a twist angle θ. The θ is measured by an autocollimator with a 5-mm-diameter reflector mounted at the center of one face of the TM. The origin of the coordinates is at the center of the cube, and horizontal coordinates are parallel with the sides of the cube (the z-axis is along the fiber). The red circles and the blue circles represent two orthogonally placed Helmholtz coils. The TM is positioned in the central region of the two Helmholtz coils, with diameters of approximately 360 mm and 290 mm, respectively. The axes of two Helmholtz coils are along the x- and y-axes, respectively. These coils form the 2D Helmholtz coils. (b) The magnified CAD drawings of the TM and 2D Helmholtz coils. The red cylinder on the TM is the reflector.

with a calculated moment of inertia $I = 4.64\times10^{-4}\,\mathrm{kg\cdot m^2}$, is 13.83 mHz. The equation of motion of the pendulum can be written as $I\ddot{\theta}+\beta\dot{\theta}+k\theta = N_\mathrm{m}+N_\mathrm{th}$, where $k = 4\pi^2 I^2 f_0^2$ is the elastic constant of the fiber. N_m and N_th are the torques produced by the magnetic field and the thermal fluctuation, respectively. $\beta = \frac{k}{2\pi f_0}\frac{1}{Q}$ is the dissipative term of the torsion pendulum, where $Q \approx 2000$ is the quality factor of the torsion pendulum system.[26] Thanks to these specifically designed structures of the measuring instrument based on Eq. (2), the measurement of kg-level TM's $\chi(\omega)$ can be performed.

3. Experimental Results. The environmental field component $B_{\mathrm{E}y}$ at the location of the TM is $B_{\mathrm{E}y} = (33.34\pm0.02)\,\mu\mathrm{T}$ measured by a three-axis fluxgate magnetic sensor (MAG-03MS100). Then, the measurement of the $\chi(\omega)$ of the copper TM is performed. The amplitude of the $B_x(\omega)$ is set to $(120\pm0.02)\,\mu\mathrm{T}$, while B_y is set to zero (thus, $B_Y = B_{\mathrm{E}y}$). The frequencies of $B_x(\omega)$ are swept from 1 to 20 mHz. By deducting the disturbance torque with the measured χ_0, the pure torques $N_\chi(\omega) = \chi(\omega)B_x(\omega)B_Y V\mu_0^{-1}$ are obtained from the raw torque data of the torsion pendulum. The typical power spectral density (PSD) of the torque $N_\chi(\omega)$ with different $B_x(\omega)$ modulated frequencies at 1, 5, and 20 mHz is shown in Fig. 3. The torque sensitivity of the torsion pendulum is approximately $1\times10^{-11}\,\mathrm{N\cdot m/Hz^{1/2}}$ around the modulated frequency. Using the typical values $B_x = 120\,\mu\mathrm{T}$ and $B_Y = 30\,\mu\mathrm{T}$, and applying a 5-hour integration time, this sensitivity performance

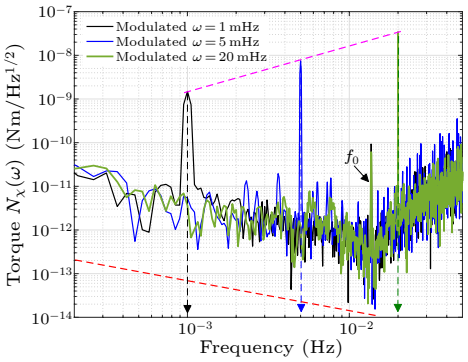

Fig. 3. The PSD of the torque $N_\chi(\omega)$ with $B_x(\omega)$ modulated frequencies at 1, 5, and 20 mHz. The black, blue, and green curves are the PSDs corresponding to the three modulated frequencies, respectively. The pink dashed line represents the connection of the $N_\chi(1\,\mathrm{mHz})$, $N_\chi(5\,\mathrm{mHz})$, and $N_\chi(20\,\mathrm{mHz})$ from three modulated experiments. The natural resonance frequency f_0 is approximately 13.83 mHz. The red dashed line shows the thermal noise limit, with a quality factor $Q = 2000$. Spectra for those 5.5-h modulated measurements are calculated with the same Hanning window.

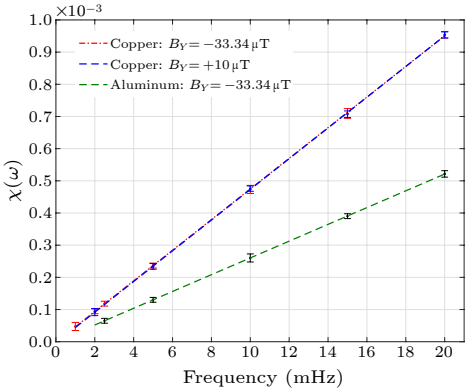

Fig. 4. The relation between $\chi(\omega)$ and ω. The red and blue dashed lines are the relations from copper data with two configurations of $B_Y = B_{\mathrm{E}y} + B_y$, respectively. The dark green dashed line is the relation from aluminium data.

results in an expected susceptibility resolution of 1×10^{-7}, which meets the required measurement resolution specified in Ref. [22].

The amplitude of $N_\chi(\omega)$ is linearly dependent on the modulated frequency ω, increasing by more than an order of magnitude from 1 to 20 mHz. It implies that $\chi(\omega)$ has the same frequency-dependent trend, since the coefficient $B_x(\omega)B_Y V\mu_0^{-1}$ in the expression of $N_\chi(\omega)$ is constant. The other modulated experiments at four interpolated ω are also performed. The relation between $\chi(\omega)$ and ω is shown in the red line of Fig. 4. The measurement is repeated by changing the magnitude of B_Y to 10 μT. The result is in excellent agreement with the result under the experimental condition of $B_Y = -33.34\,\mu\mathrm{T}$, and is also shown in Fig. 4.

By linearly fitting the data of $\chi(\omega)$ and ω, the $\chi(\omega)$ of the 5-cm-size copper TM can be given as

$$\chi_{\mathrm{Cu}}(f) = (0.047\pm0.001)f\cdot\mathrm{Hz}^{-1},\ 1\,\mathrm{mHz}\le f\le 20\,\mathrm{mHz}, \quad (3)$$

where the Hz^{-1} item is the incidental units for dimensionless $\chi(f)$. The constant term (intercept) in the fitting can

be ignored, since the term at the order of 10^{-7} is close to zero. In another configuration of the environmental field, the B_Y is set to $(10 \pm 0.04)\,\mu$T. As the blue dashed line in Fig. 4 shows, the consistent results of the $\chi_{\rm Cu}(f)$ are measured. Therefore, the $\chi_{\rm Cu}(f)$ is not related to the strength of the environmental field B_Y at a few tens μT.

We repeat the whole experiment only with the copper TM replaced by a same size aluminium (99.99% purity) TM. The configuration is set to be the same as the first configuration of the B_Y in the copper experiment. As Fig. 4 shows, the $\chi(\omega)$ of the aluminium TM is also linearly frequency-dependent, and the $\chi(\omega)$ of the aluminium TM can be given as

$$\chi_{\rm Al}(f) = (0.027 \pm 0.001) f \cdot {\rm Hz}^{-1},\ 1\,{\rm mHz} \le f \le 20\,{\rm mHz}. \quad (4)$$

The increase rate of the measured $\chi_{\rm Al}(f)$ is smaller than that of the $\chi_{\rm Cu}(f)$ due to the difference in conductivity between the aluminium and the copper cubes.

For a metal cube TM, the inside eddy currents are proportional to the conductivity σ of the TM and the magnetic permeability μ_0.[23] Given that the theoretical conductivity values of copper and aluminum are 58.5 MS/m and 37.7 MS/m, respectively, the $\chi(f)$ of 5-cm-size cubes with conductivity σ can therefore be expressed as

$$\chi_{\rm 5cm}(f) = (6.2 \pm 0.1) \times 10^{-4} \sigma \mu_0 f \cdot {\rm m}^2, \quad (5)$$

where the $\rm m^2$ item is the incidental units for dimensionless $\chi(f)$.

We reprocess the data of the $\chi(f)$ of 2-cm-size copper and aluminium cubes (the same batch and machining technique as the 5-cm-size cube) from the previous work,[22] and the $\chi(f)$ of the 2-cm-size metal cube can be modeled as

$$\chi_{\rm 2cm}(f) = (0.88 \pm 0.06) \times 10^{-4} \sigma \mu_0 f \cdot {\rm m}^2. \quad (6)$$

Since the eddy currents are proportional to the surface area L^2 of a single face of TM (L is the side length) at low frequency, the area factor L^2 should be considered in Eqs. (5) and (6). Combining the results of two torsion pendulum experiments, $\chi(f)$ can be experimentally determined as

$$\chi(f) = \chi_0 + (0.24 \pm 0.01) \sigma \mu_0 L^2 f, \quad (7)$$

where $0.1\,{\rm mHz} \le f \le 1\,{\rm Hz}$, and the χ_0 of the copper TM was measured about -1.6×10^{-6} in the previous results.[22]

4. Discussion and Conclusions. This experimentally determined $\chi(f)$ of the cube is compared with the theoretical calculations of a metal similar to the cube. Since the measured $\chi(f)$ values for metals are generally applicable, copper can be adopted as an illustration for comparison. Since the skin depths are larger than the TM size, the in-band eddy currents distribute in the whole TM volume rather than just the TM surface. Therefore, the volume parameter should be the same for both the experimentally determined and calculated $\chi(f)$.

Landau calculated the magnetic susceptibility of an isotropic conducting sphere with radius a and approximated $\chi(f) = (2\pi/10)\sigma\mu_0 a^2 f$ at low frequency.[27] Assuming the sphere has the same volume as our cube, the radius $a = \sqrt[3]{3/4\pi}\,L$ and the corresponding $\chi(f) = 0.242\sigma\mu_0 L^2 f$, which is slightly larger than the experimental equation. Chen calculated the magnetic susceptibility of conducting cylinders with radius a.[28] We set a and the ratio of bottom diameter to height to be $L/\sqrt{\pi}$ and 1 respectively, in order to approximate the volume and shape of the cube. Based on the calculated data of Chen,[28] the $\chi(f)$ of the cm-size cylinders is calculated as $\chi(f) = 0.25\sigma\mu_0 L^2 f$ below 1 Hz. Vitale first observed the frequency term of the magnetic susceptibility of TM applied in LPF and gave $\chi(f) = (\pi/12)\sigma\mu_0 L^2 f \simeq 0.262\sigma\mu_0 L^2 f$ with the f set to 1 mHz.[29] Our torsion-pendulum-based measurement results are consistent with Landau's and Chen's calculation results, showing discrepancies below 1% and 5% respectively. The discrepancy between our result and Vitale's result is below 10% at 1 mHz. This 10% discrepancy is possibly derived from the uncertainty of the adopted σ and the property difference of actual TMs in the two independent experiments.

Although the shapes of the sphere, cylinder, and cube are different, the calculated values of the sphere and cylinder are in good agreement with the determined $\chi(f)$ of the cube when their volumes are set to be the same. This indicates that the in-band eddy effect is a bulk effect, and the in-band $\chi(f)$ depends on the volume conductivity of the TM, regardless of the shape of the TM. Nevertheless, the volume conductivity σ is difficult to determine precisely due to the alloy material properties, the grabbing positioning, and the release mechanism on the TM, and so on.[30] Therefore, it is feasible to employ $\chi(f)$ with the volume conductivity of the TM cube for a preliminary estimation of the in-band eddy effect.

In LPF's latest magnetic-induced force noise calculation, the $\chi(f)$ was set as a constant value $\chi(f = 5\,{\rm mHz})$, which is the maximum value from 2 mHz to 30 mHz.[13,14] It could be a safe estimation since the variation of $\chi(f)$ of their TMs in a low enough frequency regime is tiny due to the low conductivity ($\sigma = 3.33 \times 10^6$ S/m[29]). However, $\chi(f)$ at higher frequencies (such as 1 Hz) is almost three orders of magnitude larger than $\chi(f)$ in the low enough frequency regime (mHz band). The assumption that $\chi(f)$ remains constant over the frequency band from 0.1 mHz to 1 Hz will lead to an underestimation of the in-band eddy current effects in TianQin. Different from LISA, this in-band $\chi(f)$, which varies with frequency, should be considered in TianQin. The $\chi(f)$ determined from 0.1 mHz to 1 Hz will be useful for preliminary estimation of the in-band eddy current effect in the TianQin. Additionally, this accurate measuring technique can be adopted for directly measuring $\chi(f)$ of actual kg-level TMs in other precision experiments and tests, where direct and accurate magnetic noise estimation based on $\chi(f)$ is required.

Acknowledgements. This work was supported by the National Key R&D Program of China (Grant No. 2020YFC2200500), the Key Laboratory of TianQin Project (Sun Yat-sen University), Ministry of Education, the National Natural Science Foundation of China (Grant Nos. 12075325, 12005308, and 11605065), and the Doctoral Research Foundation Project of Hubei University of Arts and Science (Grant No. kyqdf2059017).

References

[1] Amaro-Seoane P, Audley H, Babak S *et al.* 2017 arXiv:1702.00786 [astro-ph.IM]

[2] Yi Z, Gong Y, Wang B *et al.* 2021 *Phys. Rev. D* **103** 063535

[3] Wu Y L, Hu W R, Wang J Y *et al.* 2023 *Chin. J. Space Sci.* **43** 589

[4] Cai R G, Guo Z K, Hu B *et al.* 2024 *Fundam. Res.* **4** 1072

[5] Luo J, Chen L S, Duan H Z *et al.* 2016 *Class. Quantum Grav.* **33** 035010

[6] Carbone L, Cavalleri A, Dolesi R *et al.* 2003 *Phys. Rev. Lett.* **91** 151101

[7] Li H D, Gao Z Y, and Wang Z 2024 *Sci. Sin. Phys. Mech. Astron.* **54** 270406

[8] Luo J, Bai S, Bai Y Z *et al.* 2025 arXiv:2502.11328 [gr-qc]

[9] Prados C, Del Real R P, Chen D X *et al.* 1994 *Rev. Sci. Instrum.* **65** 3044

[10] Armano M, Audley H, Baird J *et al.* 2020 *Mon. Not. R. Astron. Soc.* **494** 3014

[11] Pellicer-Porres J, Lacomba-Perales R, Ruiz-Fuertes J *et al.* 2006 *Am. J. Phys.* **74** 267

[12] Xu J H, Zhang L N, Ke J *et al.* 2024 *Class. Quantum Grav.* **41** 225007

[13] Armano M, Audley H, Baird J *et al.* 2025 *Phys. Rev. Lett.* **134** 071401

[14] Armano M, Audley H, Baird J *et al.* 2025 *Phys. Rev. D* **111** 042007

[15] Qiao M N, Liu L H, Cai B S *et al.* 2023 *Chin. Phys. B* **32** 050702

[16] Antonucci F, Armano M, Audley H *et al.* 2011 *Class. Quantum Grav.* **28** 094002

[17] Quantum design: https://www.qd-china.com/en.

[18] Hueller M, Armano M, Carbone L *et al.* 2005 *Class. Quantum Grav.* **22** S521

[19] Tu H B, Bai Y Z, Zhou Z B *et al.* 2009 *Chin. Phys. Lett.* **26** 040403

[20] Yin H, Tan D Y, Hu M *et al.* 2021 *Phys. Rev. Appl.* **15** 014008

[21] Liu B, Yang Z, Qiang L *et al.* 2023 *Results Phys.* **54** 107048

[22] Xu J H, Liu Q, Luo X *et al.* 2022 *Phys. Rev. Appl.* **18** 044010

[23] Jackson J D 2012 *Classical electrodynamics* (John Wiley & Sons)

[24] Gillies G T and Ritter R C 1993 *Rev. Sci. Instrum.* **64** 283

[25] Tu L C, Li Q, Wang Q L *et al.* 2010 *Phys. Rev. D* **82** 022001

[26] Russano G 2016 arXiv:1609.00002 [physics.ins-det]

[27] Landau L D and Lifshitz E M 1984 *Electrodynamics of continuous media* (Oxford: Pergamon)

[28] Chen D X and Gu C 2005 *IEEE Trans. Magn.* **41** 2436

[29] Díaz-Aguiló M 2011 *Ph.D. Dissertation* (Universitat Politécnica de Catalunya)

[30] Vignotto D, Zanoni C, Tomasi M *et al.* 2023 *AIAA J.* **61** 5232